No. 72 December 2024

STEEL CONSTRUCTION TODAY & TOMORROW

https://www.jisf.or.jp/en/activity/sctt/index.html

Feature Article

Toward Higher Reliability of Beam-end Butt Joints

Serial Article: Latest Design of Steel Buildings in Japan (9)

Grove

Published Jointly by

The Japan Iron and Steel Federation

Japanese Society of Steel Construction

Weld Acceptance Criteria for Beam-End Butt Joints in Seismically Loaded Steel Structures

Yukihiro Harada
Professor, Chiba University

Yukihiro Harada is a professor in the Department of Architecture, Faculty of Engineering, Chiba University, Japan. He earned his Ph.D. from the University of Tokyo in 1995. His research focuses on joint design in building steel structures. Dr. Harada also chairs the special working group of the Internationalization Committee at the Japanese Society of Steel Construction, reflecting his active role in the field.

Introduction

In steel frameworks of low- and mid-rise buildings in Japan, a welded through-diaphragm-to-beam flange joint is commonly used for connecting H-shaped beams to square tube columns (Fig. 1). In the Hyogo-ken Nanbu Earthquake, brittle fractures at beam-end butt joints were observed in many steel buildings. This led to extensive investigations to prevent such fractures in beam-end welded joints[(1)]. In Japanese engineering practices, "solid tabs" are widely employed at the ends of beam-end butt joints (Fig. 2) to eliminate the need for conventional steel end tabs (also known as weld tabs or run-on/off tabs) and to smoothly finish the stress-concentrating reentrant part (Fig. 3[(2)]).

The solid tab, made from fire-resistant materials such as ceramic or flux, is a welding consumable placed at the start and end of groove welds, replacing conventional steel weld tabs. In Japan, the development of solid tabs and end tab omission method began in the 1970s to address the inefficiencies associated with conventional steel tabs[(Ex 3 and 4)]. Steel end tabs were used to contain potential welding defects at the start and end of groove welds outside the main weld, ensuring the quality of the main weld by cutting off the end tabs after welding. However, the cutting operations posed secondary risks, such as notches created by gas cutting and the hardening of the weld ends caused by short beads during tack welding. After extensive R&D, the standards for solid tabs and end tab omission method were established in the late 1980s[(5)]. Since then, the solid tab has been widely applied in building steel structures.

Although solid tabs resolved many issues associated with conventional steel tabs, some drawbacks remain. Weld defects are likely to occur at the welding ends with solid tabs because the welding starts and ends within the flange width[(6)]. These defects are difficult to inspect using conventional ultrasonic testing[(7)], and quality control of the welding ends with solid tabs was a challenge.

Fig. 1 Beam-to-Column Joint Widely Used in Japan

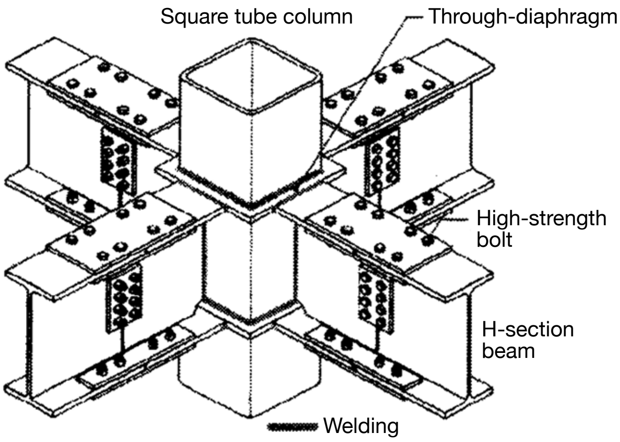

Fig. 2 Through-Diaphragm-to-Beam Flange Butt Joint

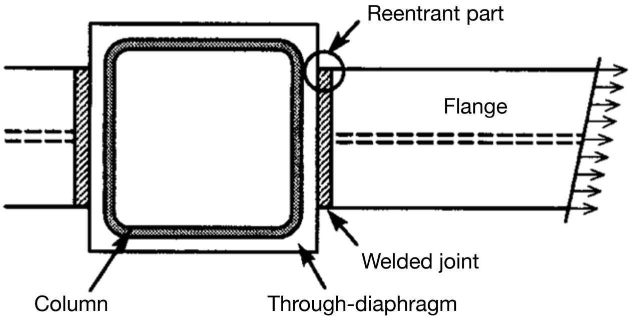

Fig. 3 Types of End Tab (adapted from Reference (2))

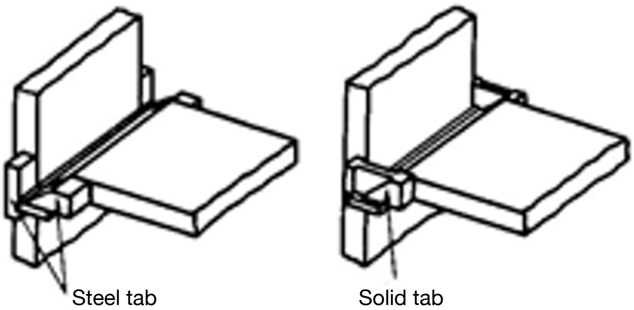

The purpose of this article is to briefly introduce the weld acceptance criteria for the welding ends of the beam-end butt joints using solid tabs; these criteria were established by a technical committee in the Japanese Society of Steel Construction[8] and later incorporated into the fourth edition of the AIJ (Architectural Institute of Japan) standard[9]. Previous experimental and analytical studies have shown that even small defects at welding ends can lead to brittle fractures, highlighting the need for supplemental inspections that measure not only the length but also the height of defects (Fig. 4). While conventional ultrasonic inspections do not require defect height measurements, this additional parameter is crucial for accurately assessing the risk of brittle fracture. By integrating knowledge of the mechanical influence of defects with advanced defect sizing techniques, the acceptance criteria for welding ends with solid tabs have been included in the AIJ standard.

Fig. 4 Possible Weld Defect at Welding End

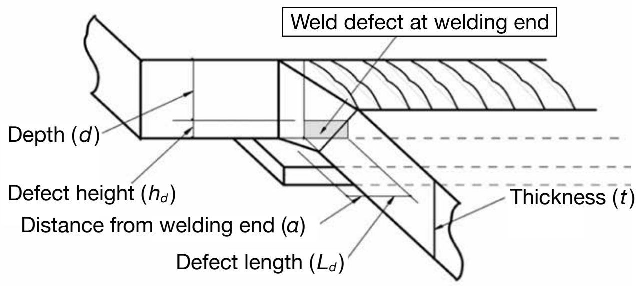

Relationship between Weld Defect Size and Butt Joint Strength

• Previous Experimental Studies

This section introduces previous experimental studies on the influence of weld defects at the ends of welded joints. Eight series of experiments were selected for discussion, including tensile-plate specimens with welded butt joints[10~13], notched tensile-plate specimens[14], beam-to-column subassemblage specimens[15~16], and beam specimens with welded butt joints[17]. In total, 86 specimens were chosen (50 for tensile tests and 36 for cyclic loading tests of beam-to-column connections). These specimens provided detailed data necessary for subsequent analytical investigation, such as weld defect size, Charpy absorbed energy of the steel material, and the size of the marginal welds.

The shapes of the selected specimens are shown in Fig. 5, and their sizes and mechanical properties are listed in Table 1. The groove was a single bevel type with a 35-degree groove angle and a 7 mm root gap. All welded joints were made using full penetration welding. The weld defects were artificial and partial (i.e., non-through-thickness) defects, created by embedding steel or copper wedges on the root face. Surface flaws in the steel plate specimens were notched using a saw blade.

Fig. 5 Test Specimens

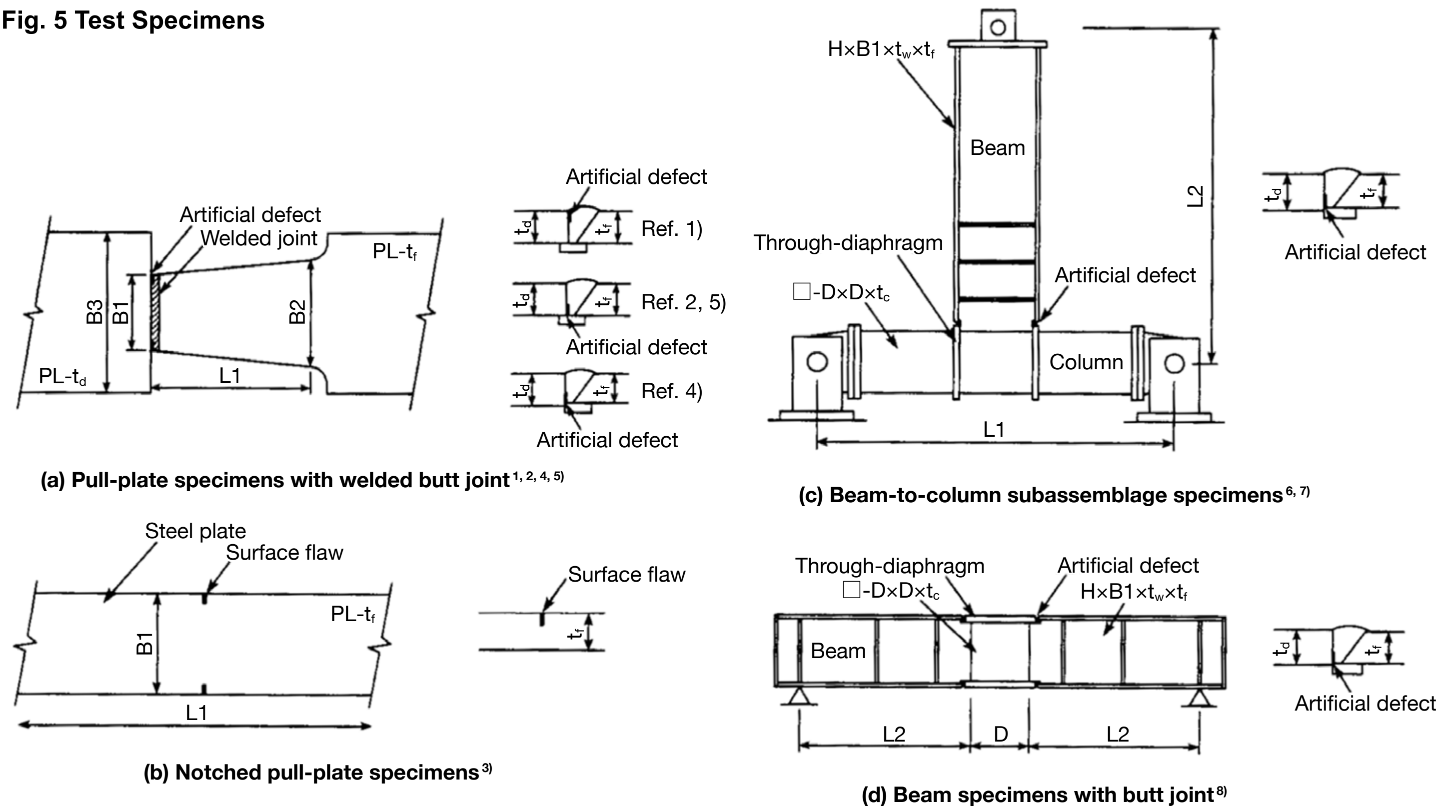

(a) Pull-plate specimens with welded butt joint [1, 2, 4, 5]

(b) Notched pull-plate specimens [3]

(c) Beam-to-column subassemblage specimens [6, 7]

(d) Beam specimens with butt joint [8]

For Ref. 1), Ref. 2, 5) and Ref. 4 and superscripts in titles, see Table 1 on the next page.

Table 1 Sizes and Mechanical Properties of Specimens

(a) Welded butt joints and steel plate

Ref	Measuring side							Fixing side					Weld metal		Remarks
	Steel	t_f	B1	B2	L1	σ_y	σ_u	Steel	t_d	B3	σ_y	σ_u	σ_y	σ_u	
1)	SN490B	19	125	180	380	381	567	SN490B	25	200	339	566	374	536	-
2)	SN490B	25	200	252	300	328	582	SN490B	25	350	328	582	460	559	L
						369	539				369	539	494	542	H
3)	SN490B	25	140	-	800	328	582	-							-
4)	SN490B	25	200	286	500	328	582	SN490B	25	480	328	582	460	559	L
						359	554				359	554	469	566	H
						321	510				321	510	529	599	A3
						361	535				361	535	529	599	A4
5)	SN490B	25	200	252	300	328	582	SN490B	25	350	328	582	460	559	-

(b) Beam-to-column connections

Ref	Beam					Diaphragm				Weld metal		Column		Remarks
	Steel	Size	L2	${}_f\sigma_y$	${}_f\sigma_u$	Steel	t_d	${}_d\sigma_y$	${}_d\sigma_u$	σ_y	σ_u	Size	Ll	
6)	SN490B	H-500×200×10×16	3500	352	535	SM490A	19	396	584	378	524	□-350×12	3000	M/M
										516	620			H/M
7)	SM490A	H-400×200×13×21	2100	369	541	SN490B	25	374	529	412	521	□-400×25	2000	FaS1, FaM1, M3
										404	520			-
8)	SM490A	H-280×200×12×22	845	381	525	SM490A	25	338	569	433	551	□-250×16	-	S
				362	530			356	520					W

L1, L2: Length of specimen (mm)
B1, B2, B3: Width of specimen (mm)
${}_f\sigma_y$: Yield stress of beam flange (N/mm²)
${}_f\sigma_u$: Tensile strength of beam flange (N/mm²)
${}_d\sigma_y$: Yield stress of diaphragm (N/mm²)
${}_d\sigma_u$: Tensile strength of diaphragm (N/mm²)
σ_y : Yield stress of weld metal (N/mm²)
σ_u : Tensile strength of weld metal (N/mm²)
t_f: Thickness of beam flange (mm)
t_d: Thickness of diaphragm (mm)

• Analytical Prediction of Butt Joint with Defects

In this study, the fracture strength of the butt joint is predicted using linear fracture mechanics[18]. The fundamental principle of linear fracture mechanics is that brittle fracture occurs when the stress intensity factor K reaches the fracture toughness K_c of the material.

According to linear fracture mechanics[19], the brittle fracture stress of a pull-plate with a through-thickness notch (Fig. 6) is expressed as follows:

$$\sigma = \frac{K_c}{F_K(\xi)\cdot\sqrt{\pi\cdot a}} \tag{1}$$

$$\xi = 2 \cdot a/B \tag{2}$$

where B is the plate width, α is the notch length, and $F_K(\xi)$ is a non-dimensional factor determined by the ratio $2a/B$. The fracture toughness K_c can be estimated as follows[20]:

$$K_c = \sqrt{\frac{2\cdot\delta_c\cdot\sigma_{yT}\cdot E}{1-\nu^2}} \tag{3}$$

$$\delta_c = F_c\left({}_vT_E,\ {}_vE_{br}/\sigma_{yT}\right) \tag{4}$$

where δ_c is the critical CTOD estimate,

Fig. 6 Pull-Plate with Through-Thickness Notch

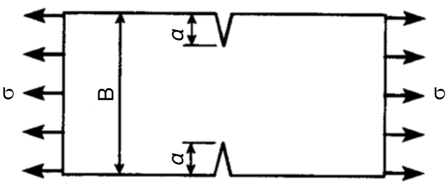

σ_{yT} is the yield stress at temperature T (°C), ${}_vE_{br}$ is the Charpy absorbed energy at the fracture point, ν is Poisson's ratio, and ${}_vT_E$ is the transition temperature (°C) of Charpy absorbed energy. The function F_c in Eq. 4 can be approximated by an exponential function of $T-{}_vT_E$[18], and the estimated fracture stress σ_{pr} is derived as follows:

$$\frac{\sigma_{pr}}{\sigma_{uT}} = \frac{341}{\sigma_{uT}} \cdot \frac{\sqrt{exp(-0.0097\cdot(T-{}_vT_E))\cdot{}_vE_{br}}}{F_K(\xi)\cdot\sqrt{\pi\cdot A_{eq}}} \tag{5}$$

$$\xi = 2 \cdot A_{eq}/B \tag{6}$$

where σ_{uT} is the maximum stress, and A_{eq} is the equivalent through-thickness flaw length defined for a partial (non-through-thickness) flaw. A_{eq} is determined so that the pull-plate with the partial flaw and the one with the through-thickness flaw have the same intensity factor K[20]. Thus, A_{eq} depends on the flaw's length a, height b, and position.

When the weld defect is small or the material's toughness is high, a ductile fracture may occur instead of a brittle fracture. The ductile fracture strength is simply determined by the product of the material's maximum stress and the joint's net sectional area, making the ratio σ_{pr}/σ_{uT} equal to the ratio of the sectional area decrease. Additionally, it is experimentally known that the strength of the butt joint is approximately 10% larger than the tensile strength of the steel material due to the restraining effect around the butt joint. When the strength increase ratio is a, the ductile fracture strength is as follows:

$$\frac{\sigma_{pr}}{\sigma_{uT}} = \alpha \cdot \frac{B-2\cdot a\cdot b/t}{B} \tag{7}$$

The fracture strength of the butt joint is predicted as the smaller value between the brittle fracture strength (Eq. 5) and the ductile fracture strength (Eq. 7).

Comparisons between the experimental fracture stress σ_{max} and the predicted stress σ_{pr}, where a is assumed to be 1.05, are shown in Fig. 7[18]. In almost all specimens, the predictions are slightly smaller than the experimental results, providing a conservative estimate.

• Relationship between Strength Decrease and Defect Size

In this section, the relationship between the strength decrease of butt joints and defect size is analytically examined based on the knowledge obtained in the previous section.

To estimate the brittle fracture stress, the transition temperature of Charpy absorbed energy ${}_vT_E$ must first be determined. In this study, the ${}_vT_E$ is estimated from the predicted Charpy energy transition curve by fitting it to a master transition curve[21]. The relationship between the Charpy absorbed energy at the fracture points at the tested temperature ${}_vE_{br}$ and the experimental $T-{}_vT_E$ is shown in Fig. 8, along with the fitted master curve of the transition. The master curve is given by the following equation:

$$ {}_vE(T) = \frac{225}{exp(-0.05\cdot(T-{}_vT_E))+1} \quad (8)$$

where ${}_vE(T)$ is the Charpy absorbed energy at temperature T. It was confirmed that the experimental results closely follow the master curve. From Eq. 8, the temperature shift $T-{}_vT_E$ can be derived as follows:

$$ T-{}_vT_E = -20\cdot ln\left(\frac{225}{{}_vE(T)}-1\right) \quad (9)$$

Using the temperature shift $T-{}_vT_E$, the brittle fracture stress in Eq. 5 can be calculated. The derived temperature shifts are shown in Table 2.

—Influence of fracture toughness of material

Fig. 9 shows the relationship between the equivalent through-thickness flaw length A_{eq} and the strength ratio γ, which is defined as σ_{pr}/σ_{uT} or σ_{max}/σ_{uT}, for varying values of ${}_vE_{br}$ at 0°C as 27, 47, and 70 J. The width of the member in the investigated weld joint is 200 mm, and the tensile strength σ_u is 490 N/mm^2. The results indicate that the maximum strength is governed by ductile fracture for smaller A_{eq}, while brittle fracture becomes the controlling factor for larger A_{eq}.

As observed in Fig. 9, the minimum A_{eq} required to induce brittle fracture increases with higher ${}_vE_{br}$ values. Consequently, the strength ratio γ also increases with larger ${}_vE_{br}$ values. Specifically, the minimum A_{eq} needed to cause brittle fracture is 12 mm when ${}_vE_{br}$ is 70 J, compared to only 5 mm when ${}_vE_{br}$ is 27 J. This highlights the importance of maintaining adequate fracture toughness of the material around butt weld joints to prevent brittle fracture.

Table 2 Estimated Temperature Shift $T-{}_vT_E$

${}_vE$(T)	27J	47J	70J
T-${}_vT_E$	-39.8	-26.6	-15.9

Fig. 7 Comparison between Experimental Results and Predictions of the Strength of the Butt Joints

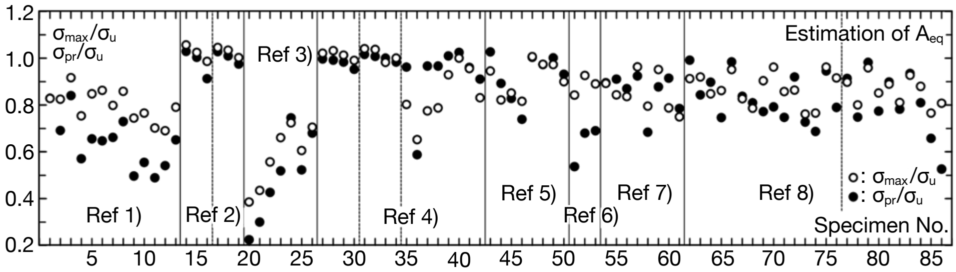

Fig. 8 Relationship between ${}_vE_{br}$ and $T-{}_vT_E$

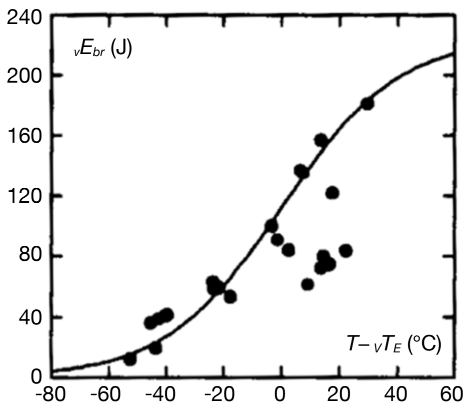

Fig. 9 Relationship between A_{eq} and Strength Ratio γ

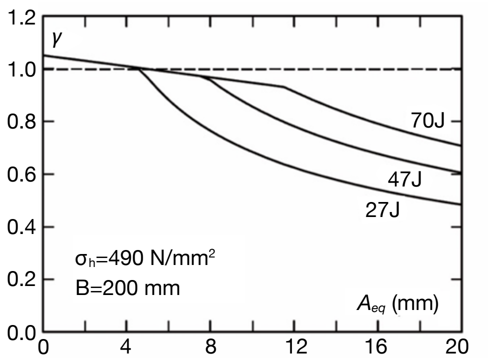

—Influence of defect size

Fig. 10 shows the relationship between defect length a and the equivalent through-thickness defect length A_{eq}, with defect height b set at 5 or 6 mm, corresponding to the bead height in the butt joint. The width of the member of the investigated joint is 200 mm, with a thickness t of either 19 or 28 mm. As expected, A_{eq} increases as the defect size whether the length a or the height b becomes larger.

Fig. 11 shows the relationships between the defect length a and the estimated strength ratio γ for different ${}_vE_{br}$ (27, 47, or 70 J) and varying thicknesses t (ranging from 16 to 40 mm). In this analysis, the defect height b is 5 mm, and the tensile strength σ_u is 540 N/mm^2. When ${}_vE_{br}$ is 27 J, brittle fracture dominates the maximum strength when the defect length a exceeds 12 mm. However, for ${}_vE_{br}$ values of 47 or 70 J, the estimated maximum strength is governed by ductile fracture, regardless of the defect length a or the thickness t. These findings provide a rough guideline for establishing weld acceptance criteria to prevent brittle fracture.

Weld Acceptance Criteria and Inspection for Beam-End Butt Joints with Solid Tabs

Based on the studies investigating the mechanical influence and inspection techniques for weld defects at the ends of butt weld joints with solid tabs, weld acceptance criteria and guidelines for supplemental inspection of the end zone in butt weld joints were proposed[8]. The guideline defines the width of the inspected end zone as 25 mm or the plate thickness t (ranging from 16 to 40 mm), whichever is larger (Fig. 12). This specification is due to the finding that 80 % of weld defects are located within 20 mm from the flange edge[6].

In the supplemental inspection, the height of the weld defect is measured using an advanced tip echo technique, which is not a part of conventional inspections. The guideline specifies allowable defect length and height, as detailed in Table 3. These acceptance criteria are divided into two categories: (a) when the Charpy absorbed energy of the heat affected zone (HAZ) in the butt weld joint ${}_vE_{br}$ is not specified, and (b) when the welding conditions are specified to ensure ${}_vE_{br}$ larger than 70 J. In the latter case (b), the allowable defect size is larger, corresponding to the higher fracture

Fig. 10. Relationship between the Length *a* and A_{eq}

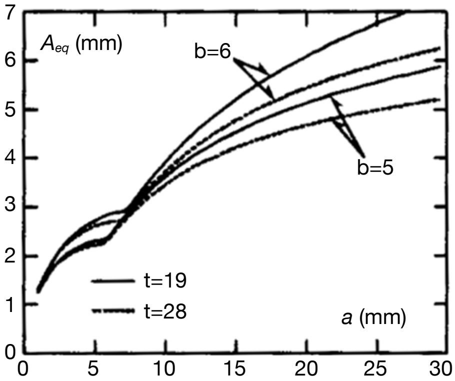

Fig. 11 Influence of Defect Size on Jjoint Strength

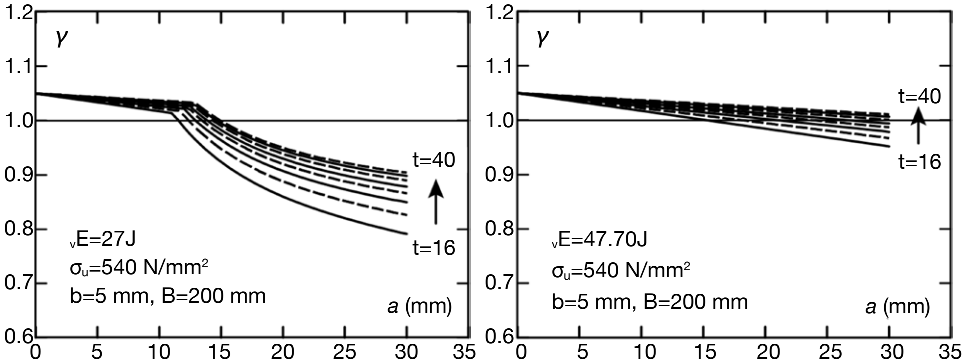

Fig. 12 Welding Ends for the Supplemental Inspection

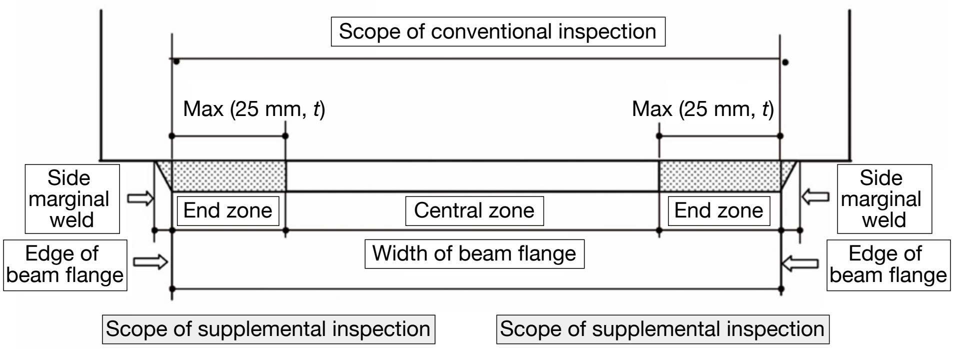

Table 3 Allowable Defect Size in the End Zone

(a) Standard case (when HAZ's ${}_vE_0$ is not specified)

Welding type and portion	Allowable limit of height	Allowable limit of length
Shop welding (upper and lower flange) Site welding (upper flange)	5 mm	12 mm
Site welding (lower flange)	5 mm	1 mm

(b) The case where HAZ's ${}_vE_0$ >70J (or expected to have equivalent toughness)

Welding type and portion	Allowable limit of height	Allowable limit of length
Shop welding (upper and lower flange) Site welding (upper flange)	5 mm	Max {l5 mm, 0.8t} (25 mm maximum)
Site welding (lower flange)	5 mm	Max {8 mm, 0.4t} (12 mm maximum)

(t: thickness of beam flange)

toughness. In the former case (a), a very small allowable defect size is specified for site welding at the lower flange due to the groove bottom being at the lowest edge of the beam, where the weld defect is subjected to high tensile stress.

The supplemental inspection is unnecessary if the beam flange width is increased at the beam-end (e.g., through the use of a horizontal haunch), thereby reducing tensile stress in the beam flange. It is important to note that controlling tensile stress, in addition to ensuring the quality of the weldment, is crucial for preventing brittle fractures at the butt joints.

References

(1) Building Center of Japan (BCJ) (2003), "Guideline for Prevention of Brittle Fracture at Beam End Welded Connections," Tokyo. (in Japanese)

(2) Japanese Society of Steel Construction (JSSC) (2007), "Fabricable Steel Design with Practical Examples," 3rd Ed. (in Japanese)

(3) K. Terai, S. Matsui, M. Kano, T. Watanabe, N. Yokoshima (1976), "Prototype and application of fire-resistant flux tab," Preprints of the National Meeting of JWS, No. 17, 250-251. (in Japanese)

(4) M. Fujimoto, Y. Kakegai, H. Terunuma, M. Obata (1978), "Welding Management and Results of the End Tab Omission Method," Annual assembly of AIJ, Structure, 1247-1248. (in Japanese)

(5) Japanese Society of Steel Construction (JSSC) (1988), "Toward Standardization of New End Tab Methods (Alternative End Tab Methods and End Tab Omission Methods)," Technical Report No. 7. (in Japanese)

(6) Building Research Institute (BRI), Japan Iron and Steel Federation (JISF), and The Japan Welding Engineering Society (JWES) (2002), "Welding Material for Steel for Building Structure and Performance of Welding Connection," Commission's report. (in Japanese)

(7) Architectural Institute of Japan (AIJ) (1996), "Standard for the ultrasonic inspection of weld defects in steel structures," 3rd Ed., Tokyo (in Japanese)

(8) Japan Society of Steel Construction (JSSC) (2008), "Guideline for Weld Acceptance Criteria and Inspection for Beam-End Butt Joints in Steel Structures," Tokyo. (in Japanese)

(9) Architectural Institute of Japan (AIJ) (2008), "Standard for the ultrasonic inspection of weld defects in steel structures," 4th Ed., Tokyo. (in Japanese)

(10) T. Suzuki, T. Ishii, K. Morita, and K. Takanashi (1999), "Experimental Study on Fracture Behavior of Welded Beam-to-column Joint with Defects," Steel Construction Engineering, 6(23), 149-164. (in Japanese)

(11) T. Hiroshige, K. Morita, K. Ishihara, M. Kato, M. Okano, T. Kojo, Y. Tsuchiya, T. Shima, and H. Hattori. (2005), "Experimental Study of Butt Joints with Surface Defects at Welding End," Annual assembly of AIJ, C-1 Structure III, 531-534. (in Japanese)

(12) C. Ozawa, T. Nakagomi, K. Hattori, Y. Ichikawa, K. Matoba, T. Kitazawa, and S. Nakamura. (2005), "Experimental Study of Butt Joints with Surface Defects at Welding End," Annual assembly of ALJ, C-1 Structure III, 543-548. (in Japanese)

(13) T. Kato, K. Morita, K. Ishihara, T. Hiroshige, M. Okano, T. Furuki, Y. Tsuchiya, and T. Shima. (2006), "Experimental Study of Butt Joints with Surface Defects at Welding End," Annual assembly of AIJ, C-1 Structure III, 977-980. (in Japanese)

(14) H. Shimokawa, T. Nakagomi, H. Okamoto, and K. Morita (2004), "Estimation of Fracture Strength Applying Linear Fracture Mechanics," Journal of Structural and Construction Engineering (Transactions of AIJ), No. 585, 169-175. (in Japanese)

(15) T. Nakagomi, K. Hattori, Y. Ichikawa, K. Matoba, and M. Iwata (2002), "Experimental Study on Deformation Capacity of Welded Beam-to-Column Connection with Weld Defects," Journal of Structural and Construction Engineering (Transactions of AIJ), No. 556, 145-150, 2002.6. (in Japanese)

(16) T. Yoshimura, M. Tabuchi, T. Tanaka, and K. Yasui (2002), "Influence of Weld Defects on Fracture of Beam-to-Column Welded Connections for Steel Frame Structures," Journal of Constructional Steel, Vol. 10, 21-26. (in Japanese)

(17) C. Ozawa, T. Nakagomi, Y. Ichikawa, T. Mutaguchi, M. Suemori. (2004), "Experimental Study on Deformation Capacity of Welded Beam-to-Column Model Connection with Weld Defects," Annual assembly of AIJ, C-1 Structure III, 569-572. (in Japanese)

(18) Shimokawa, H., Nakagomi, T., Harada, Y., Hiroshige, T., Fujita, T., Ishihara, K. and Okamoto, H. (2006), "Estimation of Fracture Strength of Butt Joints with Weld Defects," Proceedings of the 4th International Symposium on Steel Structures, 210-219.

(19) Okamura, H. (1976), "Approach of Linear Fracture Mechanics Lecture 1 of Fracture Mechanics and Material Strength," Baifukan, Tokyo. (in Japanese)

(20) The Japan Welding Engineering Society (JWES) (1997), "Method of Assessment for Flaws in Fusion Welded Joints with respect to Brittle Fracture and Fatigue Crack Growth," WES 2805:1997, Tokyo.

(21) The Japan Welding Engineering Society (2003), "Method of assessing brittle fracture in steel weldments subjected to large cyclic and dynamic strain," WES 2808:2003, Tokyo.

Defects and Plastic Deformation Capacity of Beam-end Butt Joints of Steel-frame Structures

Japanese Society of Steel Construction

In the preceding article "Weld Acceptance Criteria for Beam-End Butt Joints in Seismically Loaded Steel Structures" (see page 1), experimental studies were conducted of the influence of weld defects at the end of welded joints. In this article, with reference to the experiment results for weld acceptance criteria for butt joints introduced in the preceding article, trial examinations were made to understand the critical defect size of beam-end butt joints of steel structures from the perspective of plastic deformation capacity.

Further, the relationship between the fracture strength and the plastic deformation capacity of these joints was formularized employing an approach shown in the *Guidelines for Prevention of Brittle Fractures in Steel Frame Beam-End Welds* (The Building Center of Japan, 2003)[1] to examine the influence of welding defects on the plastic deformation capacity of beam-end butt joints.

The results of these examinations are introduced in the following:

Evaluation Parameters for Plastic Deformation Capacity

It is originally required that the allowable defect size be decided within the range in which the plastic deformation capacity required for the beam-end butt joint by the structural designer is satisfied with a certain safety factor. However, the characteristic properties of input seismic force and the structural types of building are diverse, and thus there is no established theory concerning what evaluation parameters should be applied to evaluate the plastic deformation capacity of beam-end butt joints. Fig. 1 shows the evaluation parameters for plastic deformation capacity that have been proposed so far.

In order to quantitatively evaluate the plastic deformation capacity, two approaches have been proposed so far—*Guidelines for Prevention of Brittle Fractures in Steel Frame Beam-End Welds* (The Building Center of Japan, 2003)[1] mentioned above and the *Method of Assessing Brittle Fracture in Steel Weldments Subjected to Large Cyclic and Dynamic Strain WES 2808* (The Japan Welding Engineering Society, 2003)[2]. These two approaches apply the method of giving the plastic deformation volume that imagines the skeleton curve shown in the figure. In experiments made so far, the loading test method of the cyclic incremental displacement[3] has generally been adopted, and as the method to arrange the experiment results, the skeleton curve[4] has been regarded as an effective evaluation parameter.

However, this evaluation parameter cannot be applied to a long-period seismic motion that may cause dozens of large plastic deformations over a long period[5], or the seismic motion that has

Fig. 1 Evaluation Parameters for Plastic Deformation Capacity

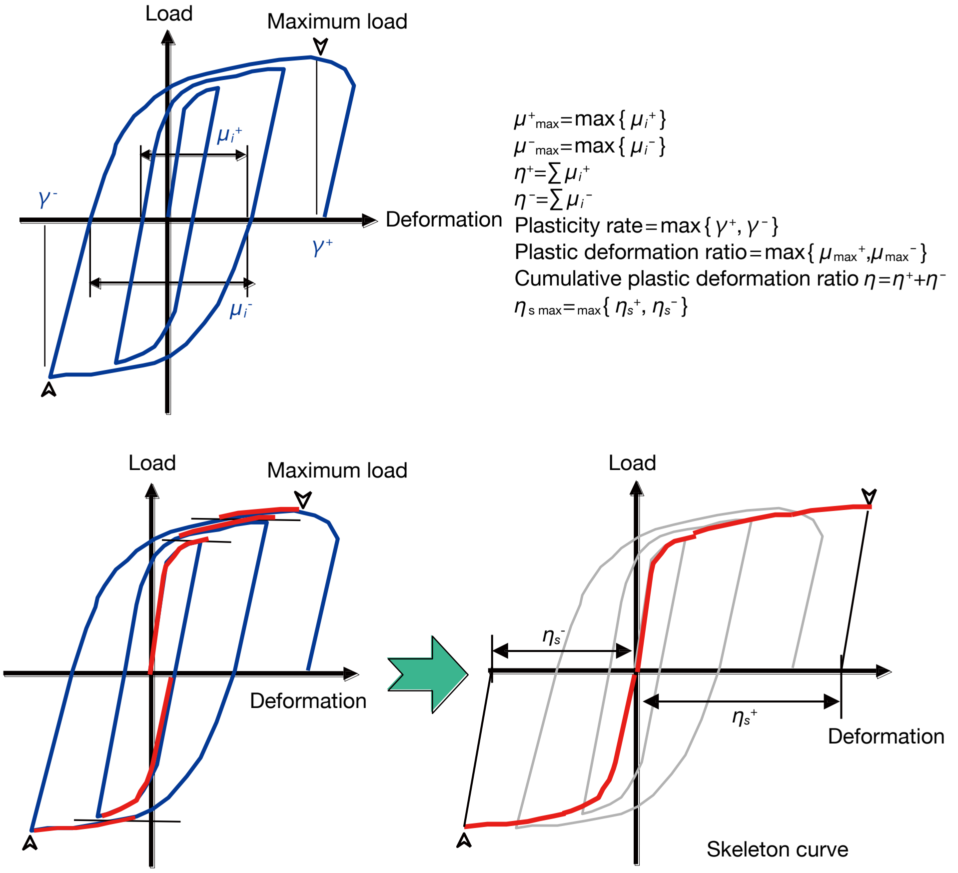

Notes to "Defects and Plastic Deformation Capacity of Beam-end Butt Joints of Steel-frame Structures"
1) The text is an exception from the "Guidelines of Ultra-sonic Test for Fracture Prevention Criteria of Welded Defect Size at Beam-End Butt Joint (JSS IV 08-2008)" published by the Japanese Society of Steel Construction.
2) Translated and published by the Japanese Society of Steel Construction.
3) Translation not guarantee. In the event of any doubt arising, the original "Guidelines" in Japanese shall take precedence.
4) Send any comments or questions about this text to the Japanese Society of Steel Construction (see back for contact details).

recently been a hot topic, and therefore it is necessary to separately examine an evaluation method for plastic deformation capacity that takes into account extremely low cyclic fatigue.

Incidentally, noticing the plastic deformation amount η_s that imagines the skeleton curve of various evaluation parameters mentioned above, the relationship between the plastic deformation capacity and the defect size was examined, and these results are introduced in this article.

Evaluation of Experiment Results

Targeting the 27 framing specimens shown in Table 1 and Fig. 2, the relationship between the defect size and plastic deformation capacity of these specimens was investigated. The table shows the dimensions of specimens and the strength of beam members, the maximum strength and the experiment results pertaining to the plastic deformation capacity.

Fig. 2 Dimensions of Specimens Used for Frame Experiment

Experiment series	Specimen dimension
B2	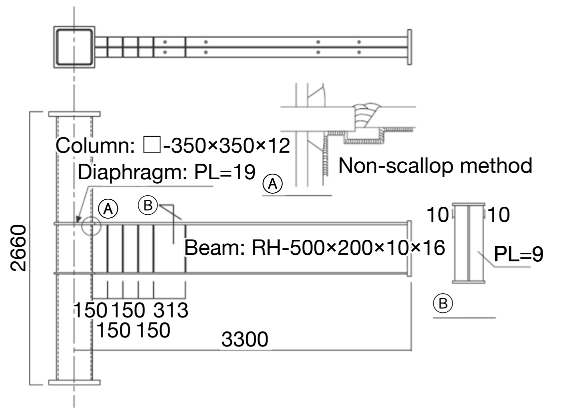
B4	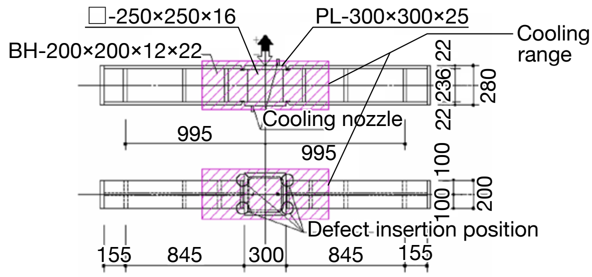

Table 1 List of Data on Maximum Strength and Plastic Deformation Capacity of Steel-frame Specimens

No.	Specimen name	Specimen dimension	Experiment results: Beam member strength			Maximum strength	Plastic deformation capacity	Joint strength	Evaluation results for plastic deformation capacity					
			$_f\sigma_y$	$_f\sigma_u$	$_w\sigma_y$	$_jM_{max}/_bM_p$	η_{smax}	γ_f	σ_y	YR	c	d	β	$_e\eta_s$
51	DBT-M/M-20		352	535	415	1.35	8.29	1.09	352	0.658	3.40	5.81	0.611	7.12
52	DBT-H/M-15	(I)	352	535	415	1.40	8.73	1.14	352	0.658	3.40	5.81	0.611	8.99
53	DBT-H/M-20		352	535	415	1.41	8.18	1.15	352	0.658	3.40	5.81	0.611	9.40
62	S_SH_5_15		381	525	432	1.54	15.70	1.18	381	0.726	4.72	6.28	1.000	14.66
63	S_SH_5_60		381	525	432	1.42	8.73	1.08	381	0.726	4.72	6.28	1.000	8.80
64	S_SH_10_30		381	525	432	1.40	7.96	1.06	381	0.726	4.72	6.28	1.000	7.85
65	S_SH_10_60		381	525	432	1.38	6.37	1.05	381	0.726	4.72	6.28	1.000	7.18
66	S_WH_5_15		381	525	432	1.54	16.57	1.19	381	0.726	4.72	6.28	1.000	15.07
67	S_WH_10_30	(II)	381	525	432	1.39	8.11	1.06	381	0.726	4.72	6.28	1.000	7.69
68	S_WH_10_60		381	525	432	1.30	5.96	0.98	381	0.726	4.72	6.28	1.000	4.65
69	S_WH_5_60		381	525	432	1.47	7.88	1.13	381	0.726	4.72	6.28	1.000	11.05
70	S_WH_5_60S		381	525	432	1.47	14.15	1.13	381	0.726	4.72	6.28	1.000	11.05
71	S_WL_5_15		381	525	432	1.53	14.44	1.17	381	0.726	4.72	6.28	1.000	14.18
73	S_WL_10_30		381	525	432	1.37	6.39	1.04	381	0.726	4.72	6.28	1.000	6.85
74	S_WL_10_60		381	525	432	1.34	5.51	1.01	381	0.726	4.72	6.28	1.000	5.86
75	W_SH_5_15		362	530	361	1.61	14.28	1.16	362	0.683	3.78	5.91	1.000	14.17
76	W_SH_5_60		362	530	361	1.54	12.95	1.11	362	0.683	3.78	5.91	1.000	10.70
77	W_SH_10_30		362	530	361	1.51	11.02	1.08	362	0.683	3.78	5.91	1.000	9.55
78	W_SH_10_60		362	530	361	1.32	5.58	0.93	362	0.683	3.78	5.91	1.000	3.99
79	W_WH_5_15		362	530	361	1.60	12.61	1.15	362	0.683	3.78	5.91	1.000	13.31
80	W_WH_5_60	(III)	362	530	361	1.47	7.28	1.05	362	0.683	3.78	5.91	1.000	8.01
81	W_WH_10_30		362	530	361	1.49	8.20	1.07	362	0.683	3.78	5.91	1.000	8.68
82	W_WH_10_60		362	530	361	1.41	7.04	1.00	362	0.683	3.78	5.91	1.000	6.04
83	W_WH_3_50		362	530	361	1.55	12.34	1.11	362	0.683	3.78	5.91	1.000	11.03
84	W_WL_5_15		362	530	361	1.61	12.73	1.16	362	0.683	3.78	5.91	1.000	13.88
85	W_WL_10_30		362	530	361	1.45	8.60	1.04	362	0.683	3.78	5.91	1.000	7.48
86	W_WL_10_60		362	530	361	1.49	7.65	1.06	362	0.683	3.78	5.91	1.000	8.55

(I) Column: □-350×12, Beam: H-500×200×10×16, Through-diaphragm PL-19×400
(II) Column: □-250×16, Beam: H-280×200×12×22, Through-diaphragm: PL-25×300
(III) Column: □-250×16, Beam: H-280×200×12×22, Through-diaphragm: PL-25×300

As to the parameter to show the maximum strength, attention was paid to the value obtained by means of dimensionless treatment of the experimental value of maximum bending moment of beam end ${}_jM_{max}$ using the full plastic moment of beam ${}_bM_p$. In addition, for the parameter of plastic deformation capacity, the skeleton curve on the positive and negative sides was found from the load-deformation hysteresis curve of beam members, and then the plastic deformation capacity was evaluated using the cumulative plastic deformation ratio $\eta_{s\ max}$ obtained by dividing the higher plastic deformation amount in the above skeleton curve by the beam deformation δ_p when the beam reaches the full plastic moment. Still more, the fracture surface of specimens after the experiment is shown in Figs. 3 and 4.

Fig. 3 Fracture Surface after Experiment (Plate Joint Experiment)

Experiment series	Specimen name	Fracture surface photo (fracture starting point)	Fracture surface photo (full view)	
A 2	L2		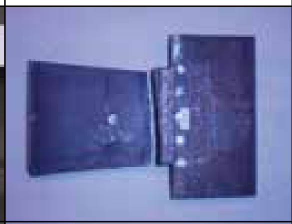	Defect height 4 mm Defect length 7 mm Fracture of heat-affected zone at bevel side
A 2	L4			Defect height 6 mm Defect length 9 mm Fracture of weld metal section
A 2	L5			Defect height 6 mm Defect length 14 mm Fracture of weld metal section
A 2	L6			Defect height 6 mm Defect length 25 mm Fracture of weld metal section

Fig. 4 Fracture Surface after Experiment (Frame Experiment)

Series/specimen name	Fracture surface photo (full view)	Fracture surface photo (detail of fracture starting point)	
B4 S_WL_5_15			Defect height 5 mm Defect length 15 mm Fracture of heat-affected zone at diaphragm side
B4 S_WH_5_60			Defect height 5 mm Defect length 60 mm Fracture of heat-affected zone at diaphragm side
B4 S_SH_10_30			Defect height 10 mm Defect length 30 mm Fracture of heat-affected zone at diaphragm side

Fig. 5 shows the relationship between the improvement rate of maximum strength ${}_jM_{max}/{}_bM_p$ after yielding and the plastic deformation capacity (cumulative plastic deformation ratio) $\eta_{s\ max}$. It can be seen from this figure that the higher the maximum strength improvement rate ${}_jM_{max}/{}_bM_p$, the higher the plastic deformation capacity $\eta_{s\ max}$. Fig. 6 shows the relationship between $\eta_{s\ max}$ and the equivalent penetrated notch length A_{eq} (see the preceding article). The figure shows the trend of the larger the A_{eq}, the lower the plastic deformation capacity.

Altogether, there were fewer experiment results in which $\eta_{s\ max}$ was 6.0 or lower. The reason why brittle fracturing did not occur at an earlier stage of experiments even when the defect was inherent in the specimen was that traces of the growth of ductile cracking from the initial-stage artificial defect were observed on the fracture surface at the stage of experiment and that the Charpy absorbed energy ${}_vE_{br}$ was comparatively high at the fracture position.

Next, the plastic deformation capacity was evaluated using the butt-joint strength coefficient γ_f, which is newly defined in this article. Specifically, γ_f is the value that is found by dividing the beam-flange's axial-direction strength P_{max} by the product obtained by multiplying the beam-flange sectional area by the flange-member tensile strength. P_{max} is the value that is found by subtracting the maximum bending moment of beam web section ${}_jM_w$ calculated by the use of the method shown in the *Recommendation for Design of Connections in Steel Structures* (The Architectural Institute of Japan, 2001) from the maximum strength of beam ${}_jM_{max}$ and by dividing the remainder by the distance between beam-flange gravity centers.

$$\gamma_f = \frac{{}_f\sigma_{max}}{{}_f\sigma_u} = \frac{P_{max}}{{}_f\sigma_u \cdot t_f \cdot B} \qquad (1)$$

$$P_{max} = \frac{\left({}_jM_{max} - {}_jM_w\right)}{d}$$

where

${}_f\sigma_u$: Tensile strength of beam-flange member (tensile test result)

t_f: Plate thickness of beam-flange member

B: Width of beam flange

Fig. 7 shows the relationship between $\eta_{s\ max}$ and γ_f. The larger the γ_f, the larger the value of $\eta_{s\ max}$, and thus it can be seen from the figure that as the strength of the butt joint becomes higher, the higher plastic deformation capacity can be obtained. In the case of examining the critical defect size that can secure plastic deformation capacity, it can be seen that this value γ_f serves as an effective parameter.

Fig. 5 Relationship between Maximum Strength ${}_jM_{max}/{}_bM_p$ and Plastic Deformation Capacity $\eta_{s\ max}$

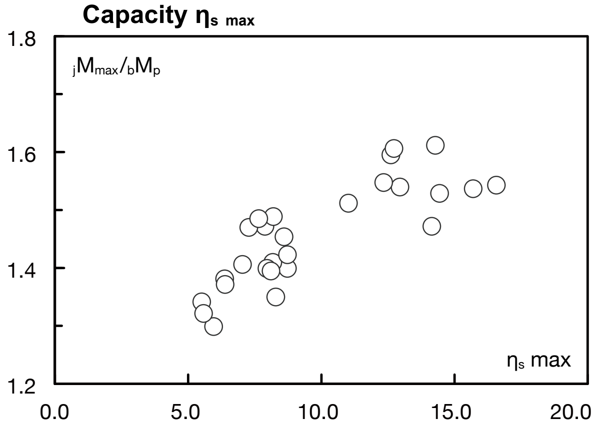

Fig. 6 Relationship between Plastic Deformation Capacity $\eta_{s\ max}$ and Equivalent Penetrated Notch Length A_{eq}

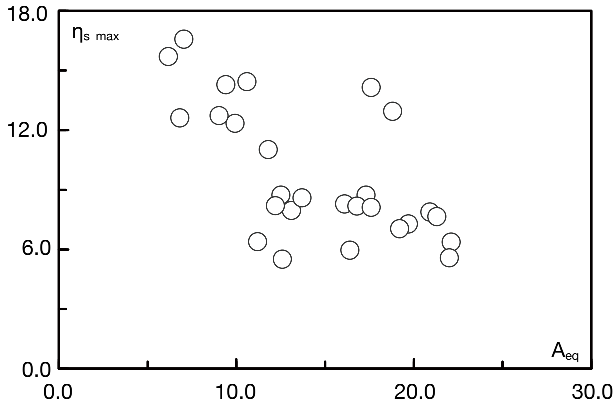

Fig. 7 Relationship between Butt-joint Strength Coefficient γ_f and Plastic Deformation Capacity $\eta_{s\ max}$

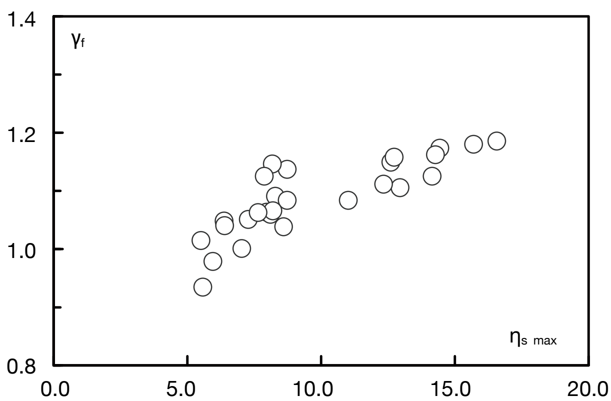

Fig. 8 shows the relationship between γ_f and the structural characteristic coefficient D_s. The value D_s was found using Equation (2).

$$D_s = 1 \Big/ \sqrt{2 \cdot \delta_{s\,\max} / \delta_p - 1} \qquad (2)$$

where

$\delta_{s\,\max}$: Maximum deformation obtained from the skeleton curve

δ_p: Deformation at the stage of full plastic strength

In the currently-prevailing structural design, D_s is mostly settled at a value between 0.2 to 0.3, and in the case of expecting the plastic deformation capacity, it is known that γ_f must be secured at 1.0 or more.

Formulization of Plastic Deformation Capacity

In the following, an attempt was made to formulize the plastic deformation capacity of beam ends having defects ${}_e\eta_s$ by applying the approach in the *Guidelines for Prevention of Brittle Fractures in Steel Frame Beam-End Welds*[1]. The plastic deformation capacity having defects ${}_e\eta_s$ was found from the following equations (3 and 4) by applying the beam member yield point σ_y, yield ratio YR, beam depth H, beam length L, beam full section plastic coefficient Z_p and plasticity coefficient only of flange section ${}_fZ_p$.

$${}_e\eta_s = \frac{{}_a\theta_{bpm} \cdot L}{\delta_p} \qquad (3)$$

$$\begin{aligned} {}_a\theta_{bpm} &= \frac{\sigma_y}{E} \cdot \frac{2L}{H} \cdot \frac{c \cdot (\alpha_1 - 1)}{(d+1) \cdot (d+2) \cdot (\alpha_0 - 1)^2 \cdot \alpha_1^{\,2}} \\ &\times \left\{ \alpha_0^{\,d+1} \cdot \left[(d+1) \cdot (\alpha_0 - 1) \cdot \alpha_1 + (\alpha_0 - \alpha_1) \right] \right. \\ &\left. - \left[(d+1) \cdot (\alpha_0 - 1) + (\alpha_0 - \alpha_1) \right] \right\} \qquad (4) \end{aligned}$$

$$\alpha_1 = \frac{\gamma_f}{YR} \cdot \frac{{}_fZ_p}{Z_p} + \beta \cdot \left(1 - \frac{{}_fZ_p}{Z_p} \right)$$

$$\alpha_0 = \frac{\gamma_f}{YR} \cdot \frac{{}_fZ_p}{Z_p} + \left(1 - \frac{{}_fZ_p}{Z_p} \right)$$

In the equation, c and d show the constants to determine the beam member moment-curvature relationship, and are values settled from σ_y and YR (refer to Table 1). In the equation, revisions were added from the settlements in Reference (1) based on the experiment results. Further, β is a coefficient that shows the effective sectional area of the beam-end web and is found using the calculation equation in Reference (6).

Fig. 9 shows the relationship between the assumed value ${}_e\eta_s$ and the experimental value $\eta_{s\,\max}$ pertaining to the plastic deformation capacity for respective specimens, which were found from Equations (3 and 4). The experimental value coincided well with the assumed value, and therefore it is considered that the fracture strength and plastic deformation capacity can be related by the use of these two equations.

Fig. 10 shows the relationship between β and YR in the case of setting γ_f=1.0. It

Fig. 8 Relationship between Butt-joint Strength Coefficient γ_f and Structural Characteristic Coefficient D_s

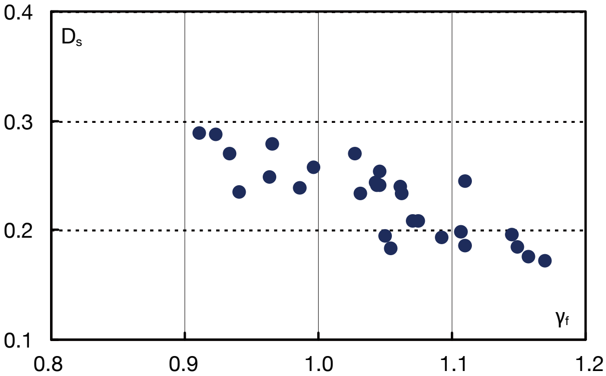

Fig. 9 Coincidence between Experimental Value $\eta_{s\,\max}$ and Assumed Value ${}_e\eta_s$ of Plastic Deformation Capacity

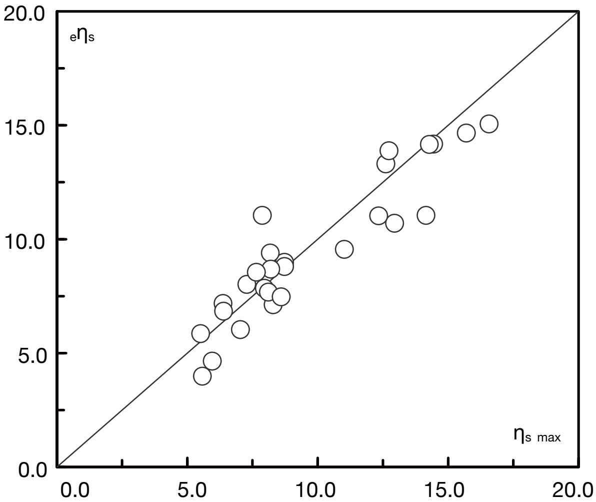

Fig. 10 Relationship between Plastic Deformation Capacity $\eta_{s\,\max}$ and Yield Ratio YR/Coefficient of Effective Sectional Area of Beam-end Web β

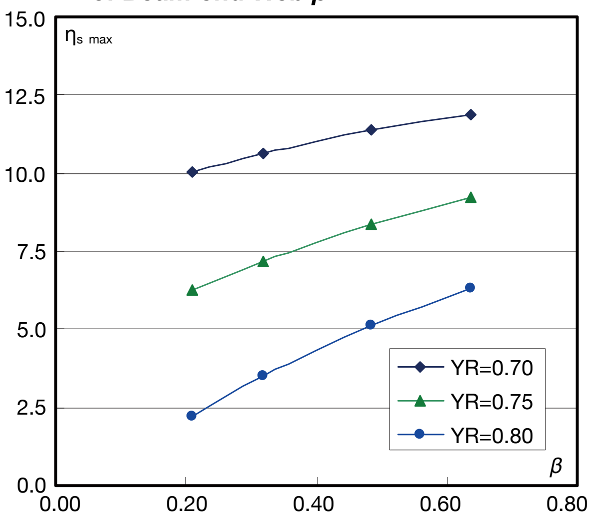

can be seen from the figure that the lower the yield ratio of the beam flange member and the larger the effective sectional area of the beam web (the effectiveness of the beam web is large), the higher the plastic deformation capacity.

Method to Settle the Critical Defect Size Based on Plastic Deformation Capacity

Once the plastic deformation capacity required for beam ends is specified, the beam-end fracture strength can be found from Equations (3 and 4) based on the specified plastic deformation capacity, and further, the critical defect size can be determined from the fracture strength using the relevant equation (see the preceding article). These approaches are considered effective as the method to judge the need or no need for the repair for weld defects confirmed by means of non-destructive inspection after weld joining.

In the following, the relationship between the plastic deformation capacity of beam ends and the fracture strength of butt joints and further, the critical defect size, was examined employing two practical examples of beam-to-column connections.

• Example of beam-to-column connection (1)

Beam: H-588×300×12×20 (SN490B)
L=4,000 mm
Column: □-400×16 (SN490C)

The necessary plastic deformation capacity ${}_r\eta_s$ was settled to its target performance for which no fracture is caused until local buckling occurs at the beam flange.

$$ {}_r\eta_s \geq \eta_0 \qquad (5) $$

Here, η_0 is found using the equation to calculate the plastic deformation capacity determined with local buckling, as proposed in Reference 7.

$$ \eta_0 = \frac{s-1}{2s^2} \cdot \left[\frac{E}{E_{st}} \cdot (s-1) \cdot (2s+1) + 3(s+1) \cdot \left(\frac{\varepsilon_p}{\varepsilon_y} \right) \right] \qquad (6) $$

$$ s^{-1} = 0.2868\lambda_f^{\,2} + 0.0588\lambda_w^{\,2} + 0.7730 $$

$$ \lambda_f = \frac{B}{2t_f} \cdot \sqrt{\frac{{}_f\sigma_y}{E}}, \quad \lambda_w = \frac{H-2t_f}{2t_w} \cdot \sqrt{\frac{{}_w\sigma_y}{E}} $$

Here, H, B, t_w and t_f are the beam depth, beam width, web thickness and flange thickness respectively, ${}_f\sigma_y$ and ${}_w\sigma_y$ are the yield points of flange and web, and E is the Young's modulus (=205,000 N/mm^2). In addition, ε_p and ε_y are the strain to start strain hardening and the yield strain respectively.

The yield point was set at ${}_f\sigma_y$=${}_w\sigma_y$=343 N/mm^2 by setting the tensile strength of the beam flange at ${}_f\sigma_u$=490 N/mm^2 and the yield ratio at YR=0.70. Further, when E/E_{st}=60 and $\varepsilon_p/\varepsilon_y$=10[7], η_0=6.35 was obtained, and ${}_r\eta_s$=6.4 was calculated.

Meanwhile, the relationship between γ_f and ${}_e\eta_s$ was found using Equations (3 and 4). β in Equation (4) differed depending on not only the diameter-to-thickness ratio of columns but also whether a scallop was provided and the method of joining the beam web to the column (weld joining or high-strength bolt joining). In this Example (1), assuming the occurrence of these differences and relatively changing β, it was decided to examine their effect on the plastic deformation capacity. Fig. 11 shows the results of this examination.

In order to satisfy ${}_r\eta_s$=6.4, it was required from Fig. 11 to settle γ_f>1.02 at β=0.64 or γ_f>1.04 at β=0.21. From the results thus obtained, an acceptable A_{eq} was found by referring to the relationship between the fracture strength and the critical defect size (see the preceding article).

• Example of beam-to-column connection (2)

Beam: H-900×250×16×25 (SN490B)
L=5,500 mm
Column: □-800×16 (SN490C)

As with the above Example (1), η_0=5.85 was found from Equations (3 and 4) to establish ${}_r\eta_s$=5.9. Also in this Example (2), the relationship between γ_f and ${}_e\eta_s$ was found by changing β (see Fig. 12).

Fig. 11 Relationship between Butt-joint Strength Coefficient γ_f and Plastic Deformation Capacity of Beam End Having Defect ${}_e\eta_s$ (Example of beam-to-column connection: 1)

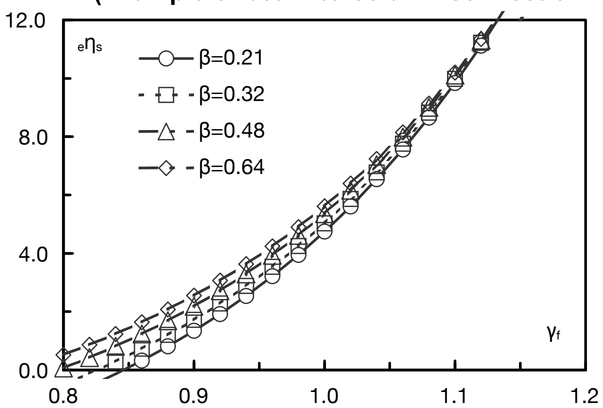

Fig. 12 Relationship between Butt-joint Strength Coefficient γ_f and Plastic Deformation Capacity of Beam End Having Defect ${}_e\eta_s$ (Example of beam-to-column connection: 2)

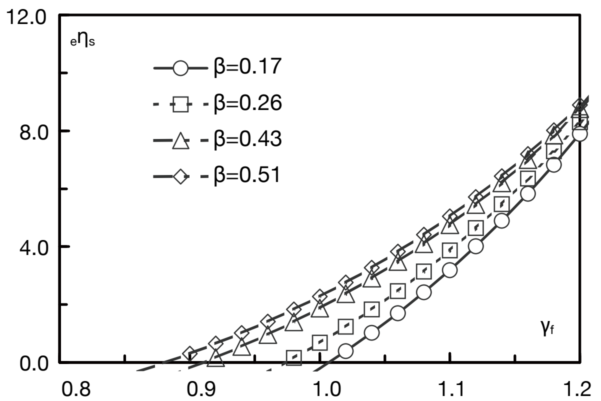

The value of γ_f in Example (2), set to satisfy an ${}_r\eta_s$ similar to that in Example (1), became considerably larger than that in Example (1) (see Fig. 12). This was due to the high ratio of the web section to the full beam section of the beam member. Further in the case of a smaller β, such as that seen in site-welded butt joints for beam ends (where web bolt connections cause sliding at an earlier stage of welding), it was seen from Fig. 12 that $\gamma_f > 1.13$ is necessary to secure ${}_r\eta_s = 5.9$. Even when the restraint effect of beam ends was expected, it was difficult to secure $\gamma_f > 1.13$. To that end, it was judged difficult to ensure the necessary plastic deformation capacity even in weld butt joints with no inherent defect.

In this way, the effect of the beam-end joining detail on plastic deformation capacity was large, as with the effect of weld joint defects, and therefore it is necessary to pay full attention to the joining detail in connection designs to prevent beam-end fractures from occurring.

Allowable Defect Sizes for Site Welding-type Beam-end Connections

It was shown in the preceding article that the plastic deformation capacity of site-welded butt joints became lower than that of shop-welded butt joints. This was due to the fact that an inside groove was prepared in the case of site-welded butt joints, so the initial layer where defects occur was subject to greater stress than in the case of shop-welded butt joints. In addition, it was assumed in the case of site-welded butt joints that high-level bending-moment transmission capacity could not be expected for the beam web due to earlier-stage sliding of the beam web bolt connection and small out-of-plane rigidity of the panel inner column flange connection where shear plates are attached, and it was considered that additional stress works on the initial layer of the lower flange.

Fig. 13 shows the evaluation results for plastic deformation capacity obtained from the existing experiment results[(8)~(15)] using the beam flange yield ratio YR and the ratio of beam-web bending moment to the bending moment of the entire beam M_{wp}/M_p as the evaluation parameters. η_f in the axial axis shows the cumulative plastic deformation ratio at the cyclic loading side where fracturing occurred. It can be seen from the figure that there is a case in which η_f falls short of 10 when YR is large or M_{wp}/M_p is large.

In this *Guidelines* (see Notes on 7), the allowable defect size in the case of site-welded butt joints was set to the stricter level than that for shop-welded butt joints by taking into account the above-mentioned evaluation results and the higher sensitivity to fracturing of the initial-layer defect[(12)] in the case of shop-welded butt joints because of the inside groove prepared in the lower flange.

The beam-end details in the case of site-welded butt joints should not easily be adopted, and in cases when this beam-end detail will be adopted, it will be necessary to make due design considerations such as the provision of haunches at the beam end. In addition, the selection of welding materials, control of welding conditions (pass-to-pass temperature, heat input) and management of the skills of welding engineers will become important.

Fig. 13 Relationship between Cumulative Plastic Deformation Ratio ηf and Yield Ratio (YR)/Ratio of Beam-web Bending Moment to Entire Beam Bending Moment (M_{wp}/M_p)$^{1/4}$

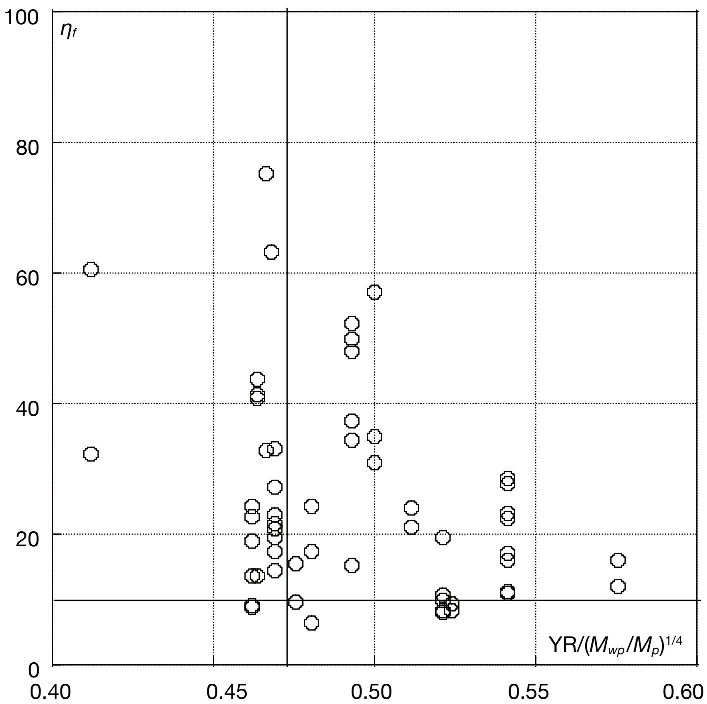

References

(1) The Building Center of Japan: Guidelines for Prevention of Brittle Fractures in Steel Frame Beam-End Welds, September 2003

(2) The Japan Welding Engineering Society: WES 2808-2000, Method of Assessing Brittle Fracture in Steel Weldments Subjected to Large Cyclic and Dynamic Strain, November 2003

(3) Building Research Institute and The Japan Iron and Steel Federation: Report of Research Committee on Structural Performance Evaluation/Testing Methods for Steel Structures, April 2004

(4) Architectural Institute of Japan: Current State of Dynamical Performance of Connections in Steel Structures, 1993

(5) Takemura, Iwata, Kagawa and Sato: Study Scientifically the Tremore of Earthquake, The University of Tokyo Press, July 2006

(6) Architectural Institute of Japan: Recommendations for Design of Connections in Steel Structures, November 2001

(7) Kato: Improvement of the Strength and Deformability of Beam-to-Column Moment Resisting Connection, Steel Construction Engineering of Japanese Society of Steel Construction, Vol. 5, No. 17, pp. 141-147, March 1998

(8) Morita, Ishii, Tada, Nakagome and Sugimoto: Fracture Behavior of Beam-to-Column Connections with Low Toughness Steel (Parts 3 and 4), Summaries of Technical Papers of Annual Meeting of Architectural Institute of Japan, C-1, pp. 411-414, September 1998

(9) Nakagome, Yamada, Ichikawa, Matoba and Murai: Experimental Study on Structural Behavior of Beam-to-Column Welded Connection Using SA440, Journal of Structural and Construction Engineering of Architectural Institute of Japan, No. 515, pp. 131-138, January 1999

(10) Steel Structure Subcommittee, Kinki Chapter, Architectural Institute of Japan: Full-Scale Test on Plastic Rotation Capacity of Steel Wide-Flange Beams Connected with Square Tube Steel Column, July 1997

(11) Nukui, Yokoyama, Sakamoto, Saraumi, Yakushiji and Tsuchida: Structural Behaviors of Plastic Hinge Region Controlled Steel Beam-Ends at Beam-to-Column Connections Welded on Site, Parts 1~3, Outline of Loading tests, 1~3, Summaries of Technical Papers of Annual Meeting of Architectural Institute of Japan, Structure III, pp. 793-798, September 2001

(12) Sakamoto, Yabe and Mase: Structural Behaviors of H−Shaped Steel Beams At Beam−to−Column Connections Welded on Site, Journal of Structural and Construction Engineering of Architectural Institute of Japan, No. 456, pp. 69-79, February 1994

(13) Tateyama: Experimental Study on the Structural Behavior of Steel Beam Welded to Column on the Site, Report of Research, Kinki Chapter of Architectural Institute of Japan, pp. 217-220, June 1993

(14) Nakagome, Fujita, Tanaka and Narusawa: Dynamic Performance of On-site Weld Type Beam-to-Column Connection, JSSC (Japanese Society of Steel Construction) Journal of Constructional Steel, pp. 101-108, July 1993

(15) Sakamoto and Yabe: Flexural Strength of Beam End in Beam-to-Column Connection of On-site Weld Joining Type, JSSC (Japanese Society of Steel Construction) Journal of Constructional Steel, pp. 337-344, November 1994

Serial Article: Latest Design of Steel Buildings in Japan (9)

Grove

—Creating Free Space in a Rigid Steel Frame Structure—

Ryu Mitarai & Associates, Architects

Working Out of New Layered Architecture

"Grove" is a multi-purpose facility composed of shops, rental housing and residences. It was built in Tokorozawa, Saitama Prefecture. In an exposed steel column-beam framing, spaces with diverse volumes are brought about as if they are entangled in the steel framing. Because of the adoption of a rigid steel-frame structure, the walls are arranged without being restricted by the framing structure, and as a result, free, bright space with large openings and an atrium is created there.

The construction site is located along the old street near Tokorozawa Station, where tile-roofed shops have ranged from long ago. While the site used to be a town arranged on long and narrow lots facing the street, the townscape was replaced due to the recent conversion into a residential area and has now been changed into the landscape of high-rise apartment buildings standing in a row. The Grove building was planned at a narrow site with a width of 9.1 m and a depth of 38.4 m that remained in the old street.

When looking around the surrounding area, several high-rise apartment buildings have been constructed and the uniform scenery is spread out with lines of identical windows of high-rise apartment buildings. Instead, in order to make the area a little more freely familiar with the environment, we examined the issue of how the newly-built layered architecture should be configured under such site conditions, which led to the start of this project.

In the building, the first and second floors are for shops, the third and fourth floors for maisonette-type rental housing and the fifth to seventh floors for dwelling units. A spacious atrium is provided through the lower three floors. Because the site is long and narrow, if the ambience inside the completed building would become dark in the rear of the building, light and wind would not be able to pass through. Therefore, we studied how to bring the traffic flow all the way around to the rear to avoid creating a back side to the building as much as possible, and to create a bright space at the foot of the approach.

Adoption of Rigid-frame Structure

When seismic-resistant elements such as walls and braces were applied in the building, structural restraints would in-

Location of Grove

PHOTO BY KAI NAKAMURA

Southside view: The lower-floor section is made wide open, and the space is piled up within the beam-column structure while changing its volume.

evitably occur above and below these elements. In order not to be restricted by these restraints, we proposed at the first discussion meeting a structural plan where the building would be constructed by the use of a rigid-frame structure.

When looking at an entire building structure, the houses and shops are built within the column/beam-structured rigid framing, giving the impression of a town just as it rises up from the ground.

Zig-zag Arrangement of Columns

For a road frontage of 9.8 m, columns are commonly arranged in two rows or three rows. In this project, the architect designer considered a four-row column structure from the start of the project. In the case of erecting the building framing with the rigid frame structure, when the columns are orderly arranged on the grid in X-Y directions, a highly uniform and encircled space is produced. In this project however, the columns were arranged in a zigzag position so that a connection with the outside could be created as much as possible. The two-row columns arranged in the center were 600-mm square tube columns or 600 mm-diameter round tube columns, and those arranged in the periphery were 300-mm square tube columns or 355 mm-diameter round tube columns.

A structural system was adopted in which bold columns were installed in the center in such a grid configuration and slightly more slender columns were installed in the periphery to support the bold columns. The lower three floors were structured as an atrium. Naturally, how to treat the seismic force is the most important factor in the rigid frame structure, and further the lower floor section in this building, which is subjected to the most severe seismic force, was structured as a three-layer atrium. Given such a situation, when the lower-floor section is constructed with a rigid frame structure, the cross section of columns would have to be quite large, and it was assumed in the initial stage that the building would be constructed with an SRC structure (steel and reinforced-concrete composite structure).

Suppression of Quake-induced Overturning with Peripheral Sub-framing

In this project, we decided to try using a steel frame structure by squeezing the cost for fireproof coating out of the construction budget. In the initial estimate, the required size of the square tube columns to be erected in the center was 1,100 mm.

In a practical sense, raising 1,100-mm square tube columns to the upper floors was thought to require a cross-section of that size, because the lower floor is not only composed of an atrium structure but also subjected to larger seismic force. However, because the upper-floor section was properly assembled with a rigid frame structure, such a large cross-section was unnecessary for the columns. In particular, we discussed the reduction of the column size for the upper floor.

When looking at the entire building remotely, the continuously-arranged columns can be seen, which seems to be a feature of this building. Therefore, it was decided not to change the size of the columns but to decrease the number of columns to be arranged in the upper-floor section.

Floor Plan

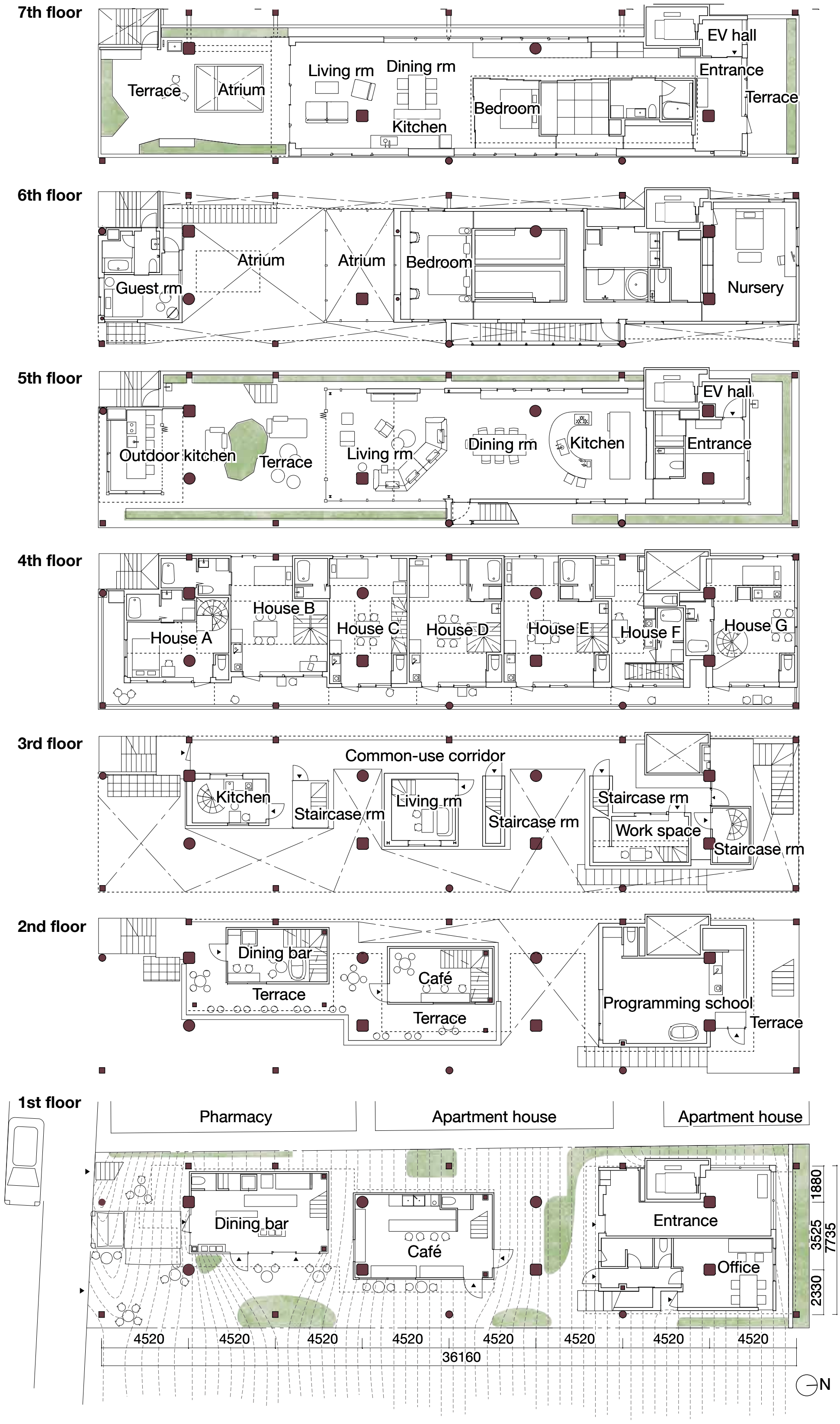

In the case of erecting columns with an identical size from the lower-floor section to the upper-floor section, steel tubes can be applied by adjusting the tube thickness without changing the outer diameter, and therefore a steel frame structure rather than the SRC structure was suitable for the construction of this building.

In the initial manual calculation, because a seismic design was examined in which the seismic force would be borne by the very short 1-span main frame, it was required for the steel tube column to have a size of 1,100-mm diameter from the aspect of securing the structural stiffness. Then, when examining the behavior of the building structure in the event of an earthquake, we discussed the possibility of using not only the main frame but also a sub-frame for the treatment of seismic force.

At the same time, when the outer sub-frame is made to work in the same way as the main frame in a rigid frame structure, the dimensions of the sub-frame will inevitably increase. In order to reduce the dimensions of the outer sub-frame in contrast to that of main frame, the sub-frame was made to work as the support for the main frame for the overturning moment in the event of an earthquake so as to complement the flexural stiffness of the main frame in the center. Based on this concept, the dimensions of the main frame could be reduced.

Space Made Available Just by Steel Structure

Generally, in a rigid frame structure, the frame is orderly aligned in the X-Y directions, and all the columns and girders in X and Y frames work for sustained vertical load. However, in terms of horizontal analysis, like X-frame only works for X-direction seismic load, the structural plane only functions in a certain direction and that from the intersecting direction does not work.

The outer sub-frame of this building is out of the grid by a factor of half from the main frame. This means that the sub-frame is not directly connected to the main frame. They are connected via an intersecting girder in order to prevent overturning during an earthquake. Due to this half-out of the grid structure, the girder in long side-direction, which usually does not do much work in the short side-direction from seismic force, is arranged to simultaneously work for the prevention of overturning. All frame members regardless of X-Y directions contribute to the short side-direction seismic force, which is cited as a weakest point of this rigid frame structures.

Further, the column supports the floor over a long run, so if the column in the upper section of main frame would be eliminated, the floor span would increase by two times, leading to the requirement for large-span beams. However, because the road frontage in this building is narrow, even when the upper section of main frame columns would be eliminated, there is another column very close opposite, so it does not mean that the beam span doubles abruptly to 18 m. That is, the span was designed in a way to make the cantilever structure effective.

Space Triggered by Columns and Beams

When the necessary floor was first considered, we settled on five floors. However, taking into account the high possibility that another building would be built on the adjacent site in the future and the accompanying deterioration of ventilation and lighting environments, we proposed raising the number of floors to seven floors. Putting this proposition into effect would create an outdoor space equivalent to about a half of the volume of the building. While this was a highly

Structure Mockup

The building structure is composed of the main frame (red) and the sub-frame (blue).

PHOTO BY KAI NAKAMURA

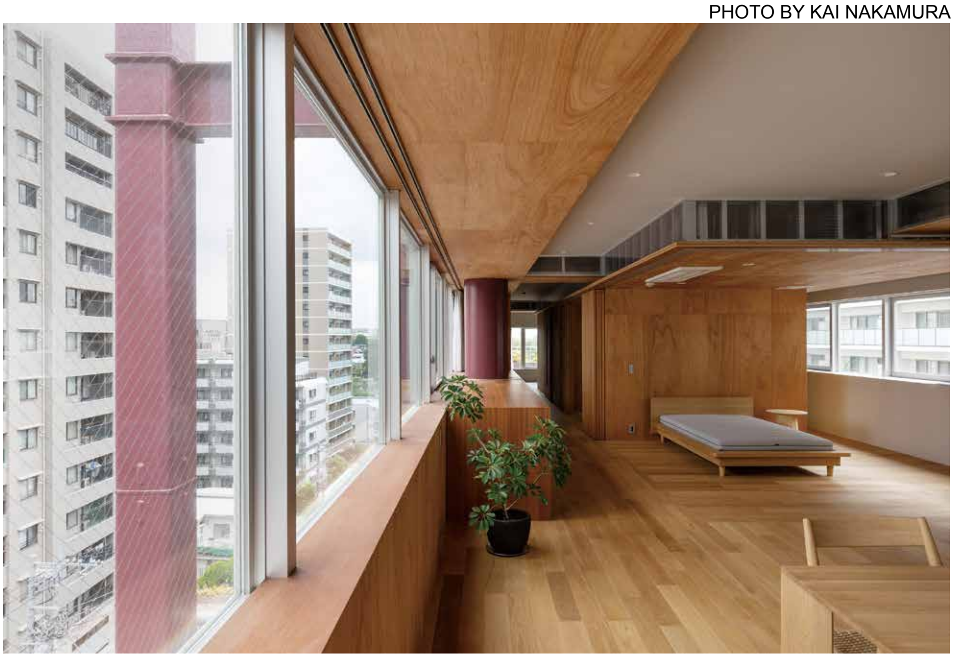

7th-floor residence: Zig-zagged columns expand the space, where beams are covered with semi-transparent polycarbonate to softly hide their installation.

challenging task for us, a building with rich openness was finally completed.

In addition, the columns and beams were arranged in an exposed form in this building, which is different from most of other buildings. In general, steel-structure buildings have columns arranged to lean closer to the outer wall or to be embedded in the wall, but in this building, the columns stand near the center of the space.

In order to make available diverse places where residents can have happy lives, the design was made so that these places were considered by properly arranging the columns and beams.

Nearly all of the columns were finished with fireproof coating and arranged intact as much as possible. The building name "Grove" means a small group of trees. In accordance with this, we aimed at realizing a space like having a stroll in a forest lined with steel-frame columns and a space that seems to have been spun out from that forest. Because finishing of all the columns with fireproof coating required a huge cost, it was decided to properly adopt fireproof cladding while examining the cost balance.

In spite of the fact that this building was constructed with a steel-frame structure, reinforced-concrete floor slabs were intentionally cast for the fourth floor, presenting an image of hanging the floor on the framing. By doing so, the building looks like a structure in which very lightweight artificial grounds have been piled up. As the exterior floor line that stands on the floor is freed from the column and beams of the building structure to some extent, the exterior terrace and the floor inside the room are integrated, leading to the creation of a space in which the inside and outside of the building are continuous.

The dimensions of the beams arranged in the lower floors were a maximum of 900 mm in height and that in the upper floors was 600 mm. The reason for the large beam height of 600 mm was that the span was nearly double and a cantilever structure was adopted because the columns were eliminated from the upper floors. The beam height could have been reduced to nearly 450 mm by changing the way of assembling columns and beams, but it was kept at 600 mm because the designers were well aware of the advantages of using a rigid frame structure, which led to the erection of strong but attractive steel-structure 'Grove' building.

Longitudinal Cross Sectional View

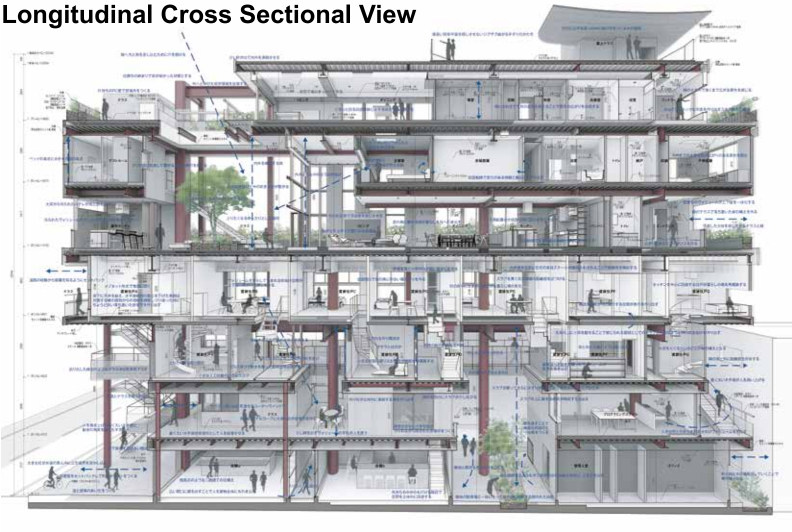

Detailed Drawing for Steel-structure Framing

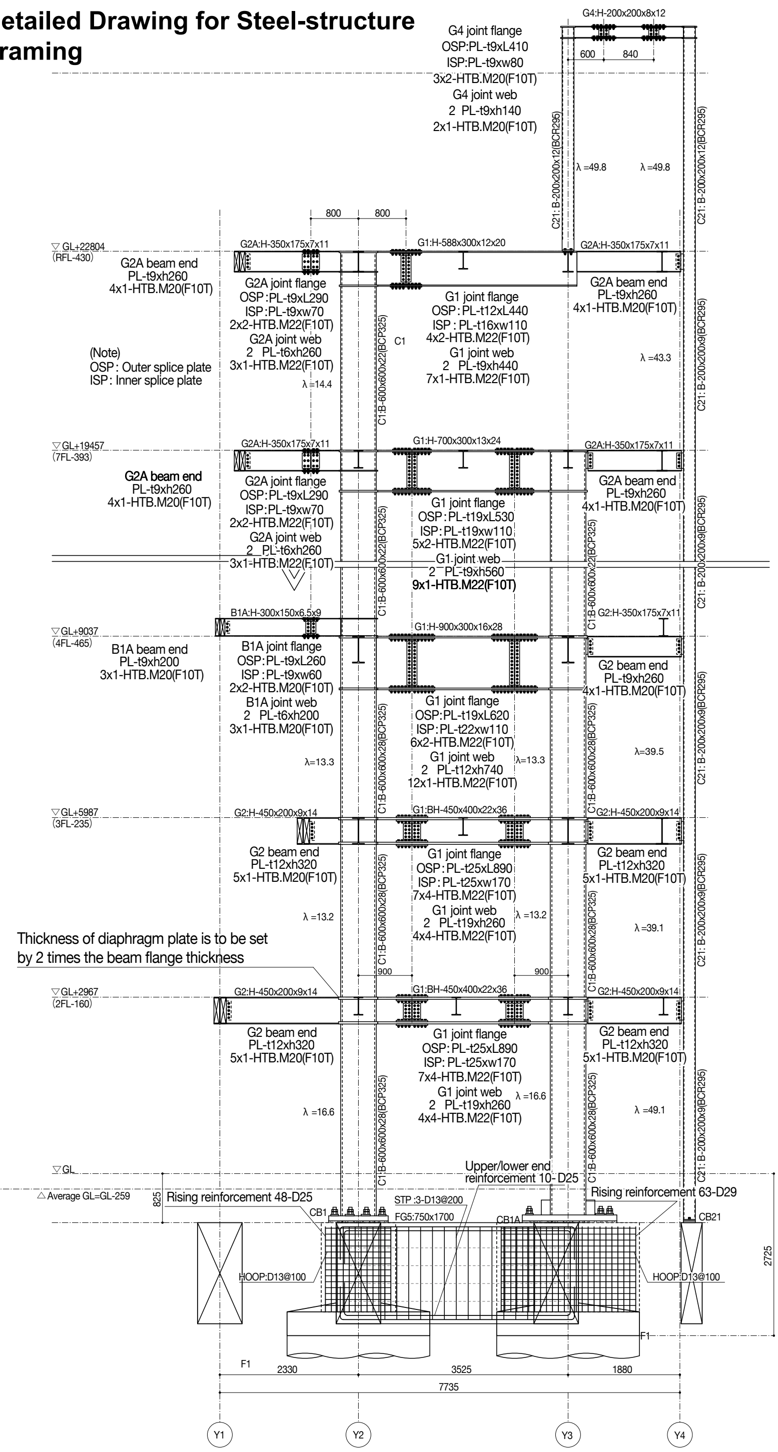

Creation of Space in Steel Framing

We thought that if originality could be applied to each column, it would bring about a sense of attachment, so we adopted both round and square steel tubes for the columns. Although there seemed to be no structural relationship between them, when walking along the first-floor approach, each of sceneries from the use of round or square tube columns seemed to be completely different. In this way, originality could successfully be applied to the structure as well.

The color adopted for the columns is another feature of the building. At first it was difficult to select the specific color for the columns. In the process of extending various studies, it was decided to apply various kinds of materials such as extruded cement board, concrete and mortar to the floor and exterior wall. Because these materials were finished with a slightly reddish grey color, we considered that this color would fit the building and offer a unique look, so it was finally decided to apply burgundy color to the columns. Capitalizing on the use of this specific color, a building was completed which provided a variety of views to be seen.

In this building, space was created in the beam-column assembled structure, and lively, comfortable living spaces were prepared. In the space prepared using the large beam height of 900 mm, when going under the beams and crossing the room, this space gives a sensation of living in a structure assembled with beams. In addition, when looking at the columns standing through the three-layer atrium, because the tops of the columns cannot be seen, there is a sensation of walking through a forest, and in the space where larch plywood is rolled up along a large beam, a slightly protected living space is arranged. In this way, we constructed the entire building structure while closely examining how to erect each column and beam.

Another theme placed on our structural design was how to connect the inside and outside of the building. The part where the roof is installed is composed of a semi-outdoor space, where an indoor space was prepared, and further inside there is also an enclosed space.

In this building, there are a total of 17 staircases, each of which is different in configuration. Because we wanted to prepare diverse types of rooms in the rental residence, each staircase was designed separately. In addition, we wanted to express affluence in the three-dimensional space, so little cost and general-purpose substrate members were applied as the finishing material. To that end, the building was completed with both carefully- and roughly-prepared members applied together. We think that these structural arrangements and materials encourage the sense of making free use of the space created in the building.

Outline of Grove

Location: Tokorozawa City, Saitama Prefecture
Project owner: DNK
Main applications: Shop, office, apartment house
Area • Site area: 335.96 m²
• Building area: 289.88 m²
• Total floor area: 1,106.39 m²
Structural type: Rigid steel frame structure
No. of stories: 7 floors aboveground, 1 penthouse
Maximum height: 23.344 m
Eaves height: 22.804 m
Architectural design: Ryu Mitarai & Associates, Architects
Structural design: HSC
Construction: Nichinan Iron Construction
Design period: May 2019~Janaury 2021
Construction period: June 2021~March 2023

PHOTO BY KAI NAKAMURA

Living room of 5th-floor residence: A large atrium connects the inside and outside of the residence and the guest room hung from the beam can be seen in the back.

PHOTO BY KAI NAKAMURA

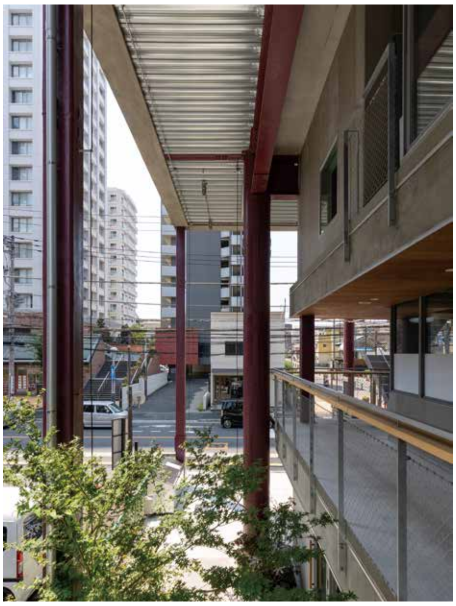

An atrium with a large entrance can be seen from the 2nd-floor terrace.

STEEL CONSTRUCTION TODAY & TOMORROW

Published jointly by

The Japan Iron and Steel Federation
3-2-10, Nihonbashi Kayabacho, Chuo-ku, Tokyo 103-0025, Japan
Phone: 81-3-3669-4815 Fax: 81-3-3667-0245
URL https://www.jisf.or.jp/en/index.html

Japanese Society of Steel Construction
3F Aminosan Kaikan Building, 3-15-8 Nihonbashi, Chuo-ku, Tokyo 103-0027, Japan
Phone: 81-3-3516-2151 Fax: 81-3-3516-2152
URL http://www.jssc.or.jp/english/index.html

Edited by
Committee on Overseas Market Promotion, The Japan Iron and Steel Federation
Chairman (Editor): Shunsuke Usami

Published three times per year, **STEEL CONSTRUCTION TODAY & TOMORROW** is circulated to interested persons, companies and public organizations to promote a better understanding of steel products and their application in the construction industry. Any part of this publication may be reproduced with our permission. To download content (PDF format), please go our website at: https://www.jisf.or.jp/en/activity/sctt/index.html. We welcome your comments about the publication and ask that you contact us at: sunpou@jisf.or.jp.